JAAS

ROYAL SOCIETY OF CHEMISTRY

TECHNICAL NOTE

View Article Online
View Journal | View Issue

Cite this: *J. Anal. At. Spectrom.*, 2025, **40**, 1645

M332 and MK617: two new potential pyrite reference materials for *in situ* sulfur isotope analysis†

Jia-Long Hao, *[a] Ruo-Long Chi,[b] Zheng-Jie Qiu, *[c] Guo-Qiang Tang,[c] Ze-Xian Cui,[d] Lian-Jun Feng,[c] Hao Yan,[e] Qiao-Qiao Zhu,[f] Ping Gao[b] and Wei Yang [a]

Received 7th March 2025
Accepted 20th May 2025

DOI: 10.1039/d5ja00089k

rsc.li/jaas

With the growing use of *in situ* techniques such as Laser Ablation Multi-Collector Inductively Coupled Plasma Mass Spectrometry (LA-MC-ICP-MS), Large Geometry Secondary Ion Mass Spectrometry (LG-SIMS), and NanoSIMS in sulfur isotope studies, new sulfide reference materials (RMs) are needed to meet increasing analytical demands and ensure accuracy. This study introduces two new natural pyrite RMs, M332 and MK617, characterized for *in situ* sulfur isotope analysis using LA-MC-ICP-MS, LG-SIMS, and NanoSIMS. Their sulfur isotope homogeneity was rigorously confirmed by *in situ* analysis, which agree with isotope Ratio Mass Spectrometry (IRMS) bulk analyses within analytical uncertainty, validating their reliability as RMs. The recommended $\delta^{34}S$ values, determined by IRMS, are 24.96 ± 0.22‰ (2 SD, $n = 10$) for M332 and −4.43 ± 0.21‰ (2 SD, $n = 12$) for MK617. Additional SIMS analyses yielded $\delta^{33}S$ values of 12.89 ± 0.60‰ (2SD, $n = 104$) for M332 and −2.23 ± 0.35‰ (2SD, $n = 120$) for MK617, further supporting their isotopic consistency. In conclusion, M332 and MK617 exhibit good isotopic homogeneity and span a wide surfur isotope range, making them highly suitable reference materials for calibrating *in situ* sulfur isotope studies across diverse geochemical and biological process applications.

1. Introduction

Sulfur, with its four stable isotopes (^{32}S, ^{33}S, ^{34}S, ^{36}S), is widely distributed in Earth's crust and serves as a key tracer in igneous, metamorphic, sedimentary, hydrothermal, and biological processes.[1–4] *In situ* sulfur isotope analysis, using techniques such as Laser Ablation Multi-Collector Inductively Coupled Plasma Mass Spectrometry (LA-MC-ICP-MS) and Secondary Ion Mass Spectrometry (SIMS), offers spatial resolution beyond that of traditional bulk methods and reveals isotopic variations within chemically heterogeneous sulfide textures.[5–10] Particularly, high-resolution techniques like NanoSIMS enable analysis of fine-grained or zoned sulfides at the micron to submicron scale.[11–14]

However, accurate *in situ* isotope analysis requires the use of matrix-matched and isotopically homogeneous reference materials (RMs) to correct for instrumental mass fractionation (IMF).[15–17] Without such standards, reliable inter-laboratory comparison and data reproducibility are difficult to achieve. Accurate calibration therefore depends on the availability of well-characterized, matrix-matched reference materials.[18,19] Given the increasing consumption of sulfide reference materials due to the expanding use of LG-SIMS and NanoSIMS, there is a continuous need to develop high-quality pyrite standards for *in situ* sulfur isotope analysis. Although recent efforts have focused on the development of sulfide RMs, including sphalerite, chalcopyrite, galena, and pyrite, for LA-MC-ICP-MS and SIMS-based applications, there remains a clear need for more widely available, homogeneous pyrite standards suitable for multiple *in situ* techniques.[20,21]

In this study, we introduce two natural pyrite samples, M332 and MK617, as new reference materials for *in situ* sulfur isotope analysis. Multi-laboratory tests using LG-SIMS, NanoSIMS, and LA-MC-ICP-MS demonstrate that these samples possess excellent $\delta^{33}S$ and $\delta^{34}S$ homogeneity, confirming their suitability for high-precision and high-resolution microanalysis. These newly developed pyrite standards are available upon request and are intended to support the global need for reliable pyrite reference standards in sulfur isotope research.

[a]*Key Laboratory of Earth and Planetary Physics, Institute of Geology and Geophysics, Chinese Academy of Sciences, Beijing 10029, China. E-mail: sean_hao@mail.iggcas.ac.cn*

[b]*School of Energy Resources, China University of Geosciences, Beijing 100083, China*

[c]*State Key Laboratory of Lithospheric and Environmental Coevolution, Institute of Geology and Geophysics, Chinese Academy of Sciences, Beijing 10029, China. E-mail: qiuzhj@mail.iggcas.ac.cn*

[d]*State Key Laboratory of Isotope Geochemistry, CAS Center for Excellence in Deep Earth Science, Guangzhou Institute of Geochemistry, Chinese Academy of Sciences, Guangzhou 510640, China*

[e]*Critical Earth Material Cycling, State Key Laboratory for Mineral Deposits Research, School of Earth Sciences and Engineering, Nanjing University, Nanjing 210023, China*

[f]*MNR Key Laboratory of Metallogeny and Mineral Assessment, Institute of Mineral Resources, CAGS, Beijing 100037, China*

† Electronic supplementary information (ESI) available. See DOI: https://doi.org/10.1039/d5ja00089k

2. Materials and methods

2.1 Sample description and preparation

Two natural pyrite samples, designated as M332 and MK617, were acquired commercially from Marin Mineral (https://www.marinmineral.com). Sample M332 (Fig. 1a) was collected from the Buick Mine, Iron County, Missouri, USA (37° 36′21″ N, 91°07′21″ W). At this locality the ore-stage pyrite forms stratabound lenses situated precisely at the lithological contact between the Bonneterre Dolomite and the overlying Lamotte Sandstone.[22] Sample MK617 (Fig. 1b) was obtained from the Merelani Hills in Arusha, Tanzania (3°33′42″ S, 36° 58′44″ E).[23]

Thin sections (1 mm thick) were first prepared from each sample. Subsequently, each specimen was cut into 10 mm diameter discs and polished on both faces for NanoSIMS and LA-ICP-MS characterization. The remaining material was subdivided into 3–4 fragments, crushed to a 40–60 mesh powder (particle size: 350–200 μm). The powder was then embedded in epoxy mounts for LG-SIMS analysis, and the mounts were polished to a flat and smooth surface with height variations of less than a few micrometers. Such surface flatness is essential to minimize instrumental artifacts, maintain consistent sputtering rates, and ensure high spatial resolution and reproducibility during microbeam analysis. The leftover 200 mesh powder was utilized for IRMS characterization.

2.2 Micro-XRF elemental analysis

Element maps of iron and sulfur were generated for two pyrite samples using the Bruker M4 TORNADO PLUS micro X-ray fluorescence (XRF) spectrometer, Institute of Geology and Geophysics, Chinese Academy of Science (IGGCAS) in Beijing, China. The Scanning μXRF experiments were carried out at the X-ray tube energy of 50 kV and a current of 600 μA, with a pixel size of 20 μm and a dwelling time of 3 ms per pixel. The Qualitative μXRF maps and quantified major elements contents were processed by Aperture Management System (AMS) software. The maps provided visual representations of the spatial distribution of Fe–S elements and the occurrence of mineral inclusions within the pyrite samples. See additional details on the experimental procedures and data analysis details from Zhang and Li (2022).[24]

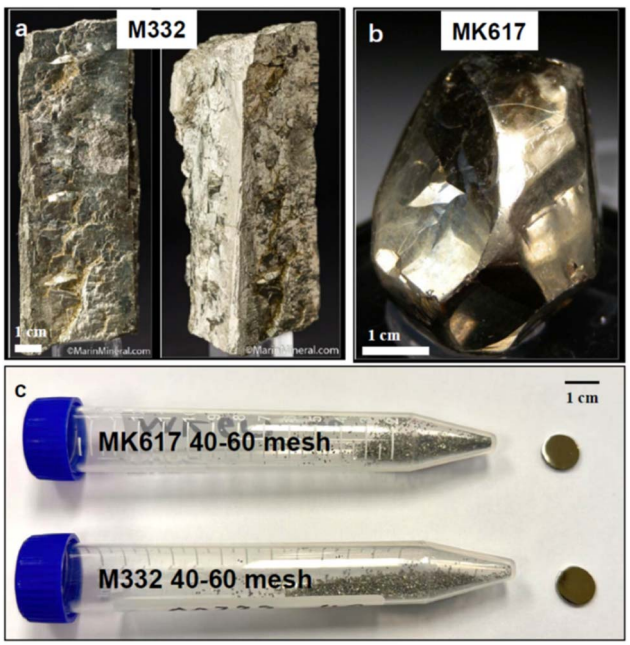

Fig. 1 The pyrite investigated in this study. (a) The hand specimen of M332 and (b) MK617. (C) Pyrite grains of 40–60 mesh and 10 mm diameter discs.

2.3 Electron probe microanalysis

The chemical homogeneity of pyrite was examined using a JEOL JXA-iHP200F electron probe microanalyzer (EPMA) at Wuhan Sample Solution Analytical Technology Co., Ltd, China. Analyses were conducted using an accelerating voltage of 20 kV, a beam current of 20 nA, and a focused beam diameter of 1 μm. Peak counting times were 10 seconds, with 5 seconds on each background. Quantitative analyses were performed using the ZAF correction method provided by JEOL. A total of eight elements (Ti, As, Zn, Cu, Ni, Co, Fe, and S) were measured using wavelength-dispersive spectrometry (WDS). The analytical setup and calibration standards were as follows: Ti (PET, TiO_2), As (TAP, FeAsS), Zn (LIFH, ZnS), Cu (LIFH, $CuFeS_2$), Ni (LIFH, $(FeNi)_9S_8$), Co (LIFH, Co metal), Fe (LIFH, $CuFeS_2$), and S (PETL, $CuFeS_2$).

2.4 IRMS sulfur isotope measurement

Sulfur isotope analysis by isotope ratio mass spectrometry (IRMS) were performed to determine the reference values of pyrite samples at two laboratories: the Laboratory for Stable Isotope Geochemistry at IGGCAS and the International Center for Isotope Effects Research (ICIER) at Nanjing University.

At IGGCAS, Pyrite sample powders (*ca.* 200 μg) and reagent V_2O_5 (*ca.* 1.6 mg) were weighed into a tin capsule, and introduced through the Finnigan Conflo IV open split interface into the Flash HT 2000 high temperature pyrolysis furnace coupled to the Thermo Scientific DELTA V Advantage mass spectrometer, where sulfide was converted to SO_2 and helium acts as carrier gas. $\delta^{34}S$ data were calibrated relative to the Vienna-Canyon Diablo Troilite scale using IAEA S1 (−0.3‰), IAEA S2 (22.65‰) and IAEA S3 (−32.5‰). Reproducibility for both sulfur-bearing analytes was ±0.3‰ (2 s). The analytical reproducibility (2SD) for replicate measurements of samples M332 and MK617 was 0.18‰ and 0.22‰, respectively.

At ICIER, sulfur isotopic compositions were determined using EA–Isolink–Delta V plus system. Approximately 0.06 mg of sample was combined with V_2O_5 and combusted at 1000 °C in an elemental analyzer and the product SO_2 was measured with a Thermo Scientific Delta V Plus isotope mass spectrometer controlled by ConFlo. The laboratory standards ICIER-S-1 and ICIER-S-2 used were calibrated by international standard samples IAEA-S-1 ($\delta^{34}S = 0.30‰$) and IAEA-S-2 ($\delta^{34}S = 22.62‰$). The analytical reproducibility (2SD) for samples of M332 and MK617 was 0.23‰ and 0.21‰, respectively.

2.5 Sulfur isotope analysis by LG-SIMS

Sulfur isotope analyses of pyrite reference materials M332 and MK617 were conducted using LG-SIMS at two laboratories: CAMECA IMS 1280 in the Institute of Geology and Geophysics, Chinese Academy of Sciences (IGGCAS), Beijing, and CAMECA IMS 1280HR in the Guangzhou Institute of Geochemistry, Chinese Academy of Sciences (GIGCAS). Both laboratories employed identical analytical conditions. A Cs^+ primary ion beam (10 kV, 2 nA) was focused in Gaussian mode to a <10 μm spot size. Secondary ions ($^{32}S^-$, $^{33}S^-$, and $^{34}S^-$) were measured simultaneously using three Faraday cups (L2p, L1, and H1) coupled with 10^{10} Ω, 10^{12} Ω and 10^{11} Ω feedback resistors, respectively. These feedback resistors balance signal intensity and noise for $^{32}S^-$ (10^{10} Ω), $^{33}S^-$ (10^{12} Ω) and $^{34}S^-$ (10^{11} Ω). Magnetic field stability was maintained *via* Nuclear Magnetic Resonance (NMR) regulation. The transfer optics magnification was set to ~133, with an entrance slit width of 110 μm and a field aperture of 4000 μm × 4000 μm. Each analysis consisted of 50 cycles with an integration time of 2 s per cycle. IMF was corrected with matrix-matched pyrite standards analyzed in the same sessions: at IGGCAS, Sonora pyrite gave $\delta^{34}S = 1.60 \pm 0.24‰$ and $\delta^{33}S = 0.80 \pm 0.38‰$ (2 SD); at GIGCAS, PPP-1 pyrite yielded $\delta^{34}S = 5.30 \pm 0.30‰$ and $\delta^{33}S = 2.73 \pm 0.20‰$ (2 SD). These in-house values agree with their published reference compositions within uncertainty and were used to correct for IMF at the respective laboratories.[25,26]

In this study, all the measured $^{34}S/^{32}S$ and $^{33}S/^{32}S$ ratios were normalized by using the Vienna Canon Diablo troilite (V-CDT) standard compositions [$^{34}S/^{32}S_{V\text{-}CDT} = (0.044163)$, $^{33}S/^{32}S_{V\text{-}CDT} = (0.007877)$]; $\delta^{34}S_{raw}$ (‰) = $[(^{34}S/^{32}S_{sample})/0.044163 - 1] \times 1000‰$, $\delta^{33}S_{raw}$ (‰) = $[(^{33}S/^{32}S_{sample})/0.007877 - 1] \times 1000‰$. All uncertainties are reported at the combined 2 SD level (σ_{total}) and include both internal precision (σ_{int}) and the propagated uncertainty of the reference material (σ_{IMF}) used for IMF correction. The total uncertainty was calculated using standard error propagation methods, as follows:

$$\sigma_{total} = \sqrt{\sigma_{int}^2 + \sigma_{IMF}^2}$$

2.6 Sulfur isotope analysis by NanoSIMS

Sulfur isotopic measurements were performed using a CAMECA NanoSIMS 50L at the NanoSIMS Lab, IGGCAS. Negative secondary ions ($^{32}S^-$, $^{33}S^-$, and $^{34}S^-$) were simultaneously detected with three Faraday cups (10^{11} Ω, 10^{12} Ω, and 10^{11} Ω resistors, respectively) using an 800 pA Cs^+ primary beam, with temperature regulation stabilizing the preamplifiers. The instrument employed Entrance Slit #3 and Aperture Slit #3 to achieve an ~80 pA (5×10^8 counts per seconds) ^{32}S intensity from pyrite. Each 10 × 10 μm^2 analysis area was pre-sputtered with a ~1 nA beam for 50 seconds to remove surface coatings and ensure stable ion yields, followed by a 300-second counting time. The pyrite standard PY-SRZK ($\delta^{34}S = 3.60 \pm 0.1‰$) was used for calibration.[18] Repeated measurements of PY-SRZK yielded a $\delta^{34}S$ value of 3.6 ± 0.50‰ (2SD) and $\delta^{34}S$ value of 1.9 ± 0.46‰ (2SD).

2.7 LA-MC-ICP-MS analysis

LA-MC-ICP-MS sulfur isotope analyses were performed on a Neptune Plus MC-ICP-MS (Thermo Fisher Scientific, Bremen, Germany) equipped with a Geolas HD excimer ArF laser ablation system (Coherent, Göttingen, Germany) at the Wuhan Sample Solution Analytical Technology Co., Ltd, Hubei, China. In the laser ablation system, helium was used as the carrier gas in the laser ablation system and was mixed with argon (makeup gas) downstream of the ablation cell. Analyses were performed in single-spot ablation mode using a 44 μm spot size and a laser repetition rate of 2 Hz. Each analysis consisted of 100 laser pulses with a laser fluence maintained at ~5 J cm^{-2} to ensure consistent ablation conditions. The Neptune Plus was equipped with nine Faraday cups fitted with 10^{11} Ω resistors. Sulfur isotopes ^{32}S and ^{34}S were simultaneously collected using L3 and H3 Faraday cups, respectively, in static collection mode. The in-house pyrite standard PPP-1 ($\delta^{34}S = 5.30 \pm 0.20‰$) was employed as the primary reference materials for mass bias correction and for monitoring instrumental stability during analysis of unknown pyrite samples. In addition, the pyrite standard SP-Py-01 ($\delta^{34}S = 2.00 \pm 0.50‰$) was employed as a secondary standard to monitor analytical accuracy. Repeated measurements of SP-Py-01 yielded a $\delta^{34}S$ value of 1.94 ± 0.40‰ (2SD, $n = 14$), which is in good agreement with its recommended value, confirming the reliability of the analytical protocol. Operating at high mass resolution (>8000), the Neptune Plus effectively resolved sulfur isotopes from potential isobaric interferences (*e.g.*, $^{64}Ni^{2+}$, $^{64}Zn^{2+}$ on $^{32}S^+$; $^{66}Zn^{2+}$ on $^{33}S^+$; $^{68}Zn^{2+}$ on $^{34}S^+$), as well as polyatomic interferences from oxygen, hydrogen, and nitrogen.

Trace element analysis of sulfides was conducted by LA-ICP-MS at the Wuhan Sample Solution Analytical Technology Co., Ltd, Wuhan, China. Laser ablation was carried out using a GeolasPro system equipped with a COMPexPro 102 ArF excimer laser (193 nm wavelength, maximum energy 200 mJ) and a MicroLas optical system. Ion-signal intensities were acquired using an Agilent 7900 ICP-MS instrument. Helium was applied as a carrier gas, while argon was introduced as the make-up gas and mixed with the carrier gas *via* a T-connector before entering the plasma. The laser spot size and repetition rate were set to 32 μm and 5 Hz, respectively. Each analysis included a 20–30 s background acquisition followed by 50 s of signal acquisition. Trace element compositions in pyrite were calibrated against the NIST SRM 610 glass standard. Data reduction was performed using the in-house developed ICPMSDataCal software, which applies matrix normalization to correct for matrix effects between the silicate standard and sulfide samples. The USGS MASS-1 sulfide reference material as an unknown to monitor analytical accuracy. The measured concentrations of trace elements in USGS MASS-1 showed good agreement with the GeoReM recommended values (http://georem.mpch-mainz.gwdg.de/), with most elements falling within ±10–15% of the accepted concentrations.

3. Results and discussion

3.1 Chemical composition of M332 and MK617

The major and trace element compositions of 40 randomly selected M332 and MK617 pyrite grains were analyzed using

EPMA. The results showed that the major element compositions of pyrite samples M332 and MK617 pyrites are fairly homogeneous (Table S1†). For M332 pyrite, the average Fe and S contents are 46.14 ± 0.15 wt% and 53.15 ± 0.16 wt%, respectively (n = 20). Similarly, MK617 pyrite shows an average Fe content of 46.05 ± 0.21 wt% and S content of 53.30 ± 0.13 wt% (n = 20). Elemental distribution maps (Fig. 2) for both samples provide a visual representation of Fe and S across the analyzed areas. These maps show no evidence of internal growth zoning, mineral inclusions, or compositional heterogeneity, further supporting their suitability as homogeneous reference materials for *in situ* sulfur isotope analysis.

Trace elements in pyrite M332 and MK617 analyzed by LA-ICP-MS are summarized in Table S2.† The results indicate that M332 exhibits generally low trace element contents, with Zn showing a moderate enrichment (mean 5.4 ppm, range 2.27–8.15 ppm). In contrast, MK617 is distinguished by elevated and notably uniform concentrations of Co (mean ~69 ppm), Ni (mean ~918 ppm), and Se (mean ~21 ppm). These contrasting elemental signatures—M332 characterized by variable Zn content and MK617 by pronounced Co–Ni–Se enrichment—highlight their complementary roles as reference materials.

3.2 Sulfur isotope determined by IRMS

Sulfur isotope measurements (δ^{34}S) were conducted using isotope ratio mass spectrometry (IRMS) at two separate laboratories, with results summarized in Table 1. For pyrite reference material M332, δ^{34}S values ranged from 24.7‰ to 25.2‰, yielding a mean of 24.96 ± 0.22‰ (2SD, n = 10). For pyrite reference material MK617, δ^{34}S values ranged from −4.58‰ to −4.21‰, with a mean of −4.43 ± 0.21‰ (2SD, n = 12).

3.3 Sulfur isotope determined by *in situ* analysis

To assess the sulfur isotope composition and homogeneity in M332 and MK617 pyrites, 264 measurements were conducted using LA-MC-ICP-MS, LG-SIMS, and NanoSIMS, with results summarized in Table 2 and Fig. 3. Detailed data are in Tables S3–S6.†

3.3.1 LA-MC-ICP-MS analysis. Twenty measurements evaluated sulfur isotope homogeneity. M332 pyrite δ^{34}S values ranged from 24.38‰ to 25.24‰ (mean: 24.70 ± 0.48‰, 2SD, n = 20), while MK617 pyrite ranged from −4.70‰ to −4.02‰ (mean: −4.43 ± 0.42‰, 2SD, n = 20).

Table 1 IRMS sulfur isotope results for M332 pyrite and MK617 pyrite

	M332	MK617
Lab.	δ^{34}S (‰)	δ^{34}S (‰)
ICIER	25.03	−4.50
	24.99	−4.21
	24.96	−4.34
	24.83	−4.46
	24.75	−4.34
	—	−4.45
	—	−4.48
Mean	24.91 ± 0.23 (2SD)	−4.40 ± 0.21 (2SD)
IGGCAS	24.99	−4.30
	24.91	−4.58
	25.15	−4.42
	25.02	−4.51
	24.97	−4.51
Mean	25.01 ± 0.18 (2SD)	−4.46 ± 0.22 (2SD)
Total mean	24.96 ± 0.22 (2SD, n = 10)	−4.43 ± 0.21 (2SD, n = 12)

3.3.2 LG-SIMS (IGGCAS). The δ^{34}S and δ^{33}S values of M332 pyrite ranged from 24.56‰ to 25.31‰ (average: 24.86 ± 0.39‰, 2SD, n = 42) and 12.72‰ to 13.58‰ (average: 13.16 ± 0.57‰, 2SD, n = 42), respectively. MK617 pyrite yielded δ^{34}S values from −4.56‰ to −4.12‰ (average: −4.33 ± 0.31‰, 2SD, n = 50) and δ^{33}S from −2.53‰ to −1.67‰ (average: −2.15 ± 0.51‰, 2SD, n = 50).

3.3.3 LG-SIMS (GIGCAS). M332 pyrite yielded mean δ^{34}S and δ^{33}S values of 24.58 ± 0.48‰ (2SD, n = 32) and 12.63 ± 0.26‰ (2SD, n = 32), respectively, while MK617 pyrite had δ^{34}S of −4.60 ± 0.35‰ (2SD, n = 40) and δ^{33}S of −2.37 ± 0.20‰ (2SD, n = 40).

3.3.4 NanoSIMS analysis. Thirty NanoSIMS measurements of M332 pyrite yielded δ^{34}S of 25.20 ± 0.56‰ (2SD, n = 30) and δ^{33}S of 12.80 ± 0.68‰ (2SD, n = 30). Similarly, thirty MK617 pyrite measurements yielded δ^{34}S of −4.21 ± 0.53‰ (2SD, n = 30) and δ^{33}S of −2.2 ± 0.58‰ (2SD, n = 30). Additionally, a δ^{33}S *versus* δ^{34}S plot (Fig. 4), incorporating all SIMS sulfur isotope data along with monitoring standards from various laboratories, yields a slope of 0.517 (n = 257, R^2 = 0.99), which is consistent with the expected mass-dependent fractionation (MDF) ratio of 0.515.[27]

3.4 Homogeneity of reference materials

Homogeneity was tested in accordance with ISO Guide 35.[28] In this test each mount or disc is treated as an individual unit; the

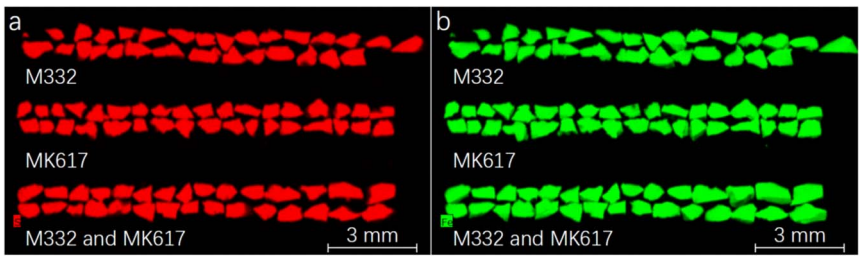

Fig. 2 Fe–S element maps of M332 and MK617 grains in epoxy mount. (a) Sulfur content mapping; (b) iron content mapping.

Table 2 Summary of mean values for sulfur isotopes ($\delta^{34}S$ and $\delta^{33}S$) obtained *in situ* determinations in M332 pyrite and MK617 pyrite

	M332						MK617					
Method	$\delta^{34}S$ (‰)	2SD	n	$\delta^{33}S$ (‰)	2SD	n	$\delta^{34}S$ (‰)	2SD	n	$\delta^{33}S$ (‰)	2SD	n
IMS 1280	24.86	0.32	42	13.16	0.42	42	−4.33	0.21	50	−2.15	0.32	50
IMS 1280 HR	24.58	0.38	32	12.63	0.22	32	−4.60	0.18	40	−2.37	0.15	40
NanoSIMS	25.20	0.25	30	12.80	0.50	30	−4.21	0.16	30	−2.19	0.35	30
LA-MC-ICP-MS	24.70	0.46	20	—	—	—	−4.43	0.40	20	—	—	—

variance among replicate spots on the same unit defines the within-unit variance (S_{within}^2), whereas the variance among unit means yields the between-unit variance ($S_{between}^2$). Specifically, an F-test—based on one-way ANOVA—was employed to compare the variances between sample units. The F ratio, defined as the ratio of the between-unit variance ($S_{between}^2$) to the within-unit variance (S_{within}^2), provides a quantitative measure of the material's homogeneity.

$$F = \frac{S_{between}^2}{S_{within}^2}$$

The between-unit variance ($S_{between}^2$) is calculated as the ratio of the between-unit sum of squares ($SS_{between}$) to its degrees of freedom ($\nu_{between}$), and the within-unit variance (S_{within}^2) is determined as the ratio of the within-unit sum of squares (SS_{within}) to its degrees of freedom (ν_{within}):

$$S_{between}^2 = \frac{SS_{between}}{\nu_{between}} \text{ and } S_{within}^2 = \frac{SS_{within}}{\nu_{within}}$$

Here, the degrees of freedom are defined by the number of sampling units (m) and the total number of replicate measurements (n):

$$\nu_{between} = m - 1,\ \nu_{within} = m\,(n - 1)$$

Table 3 summarizes the one-way ANOVA results. According to ISO Guide 35 (2017), homogeneity is designated 'excellent' when the between-unit variance is not significantly larger than the within-unit variance, *i.e.* when the ANOVA statistic satisfies

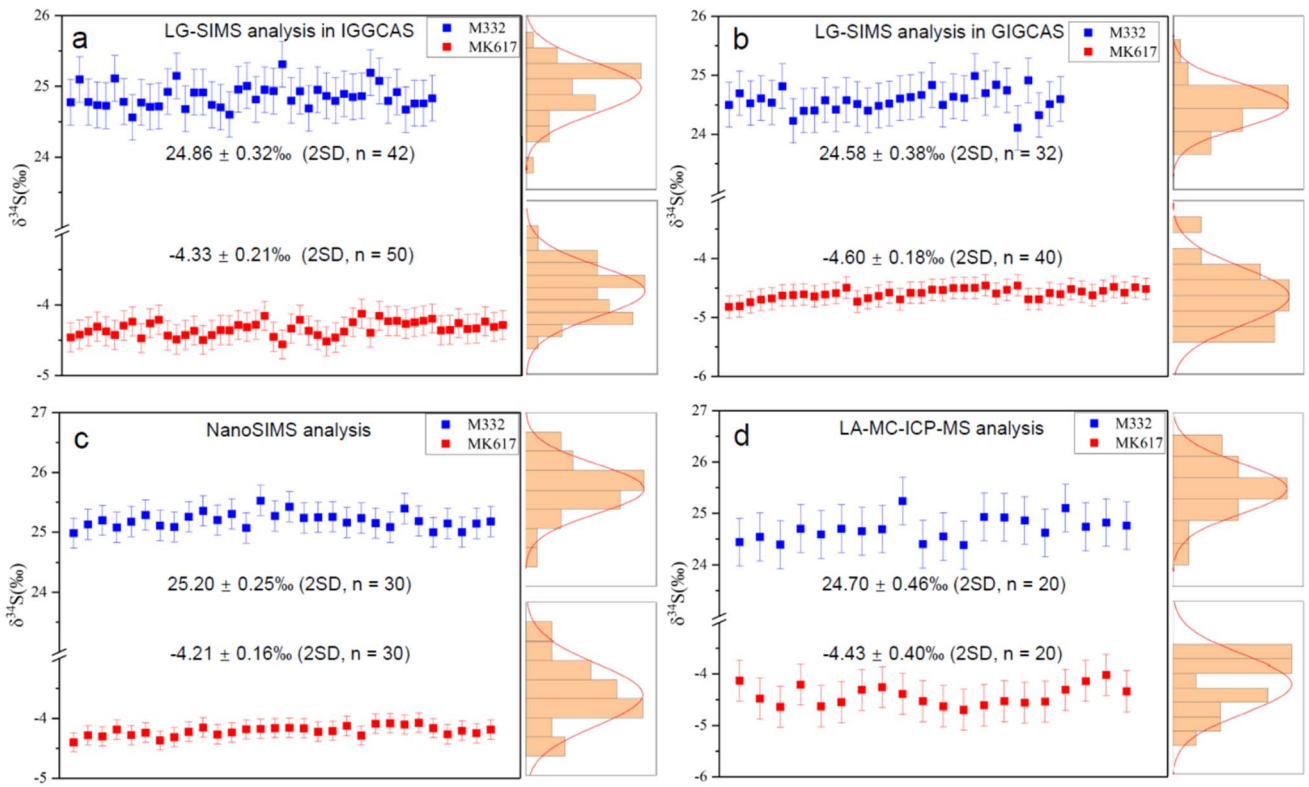

Fig. 3 Sulfur isotope compositions of M332 pyrite and MK617 pyrite. The $\delta^{34}S$ values of M332 pyrite and MK617 pyrite determined in different laboratories with the frequency histogram and the best-fit normal distribution curves.

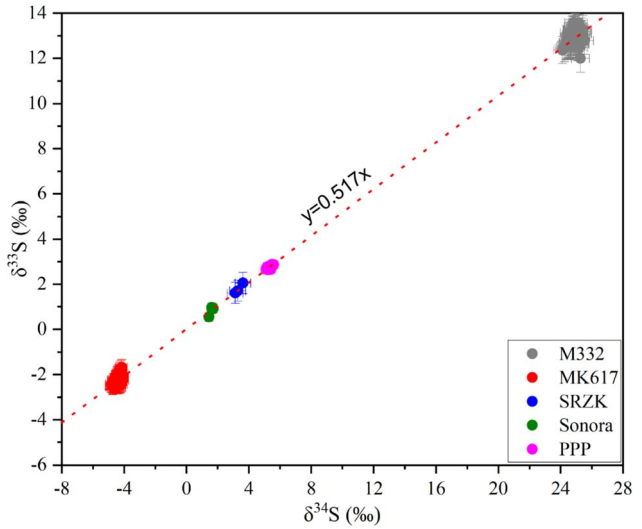

Fig. 4 Plot of $\delta^{33}S$ *vs.* $\delta^{34}S$. All the data are plotted on a near-ideal trend (red dash line). Horizontal and vertical bars represent ±2 SD of replicate measurements.

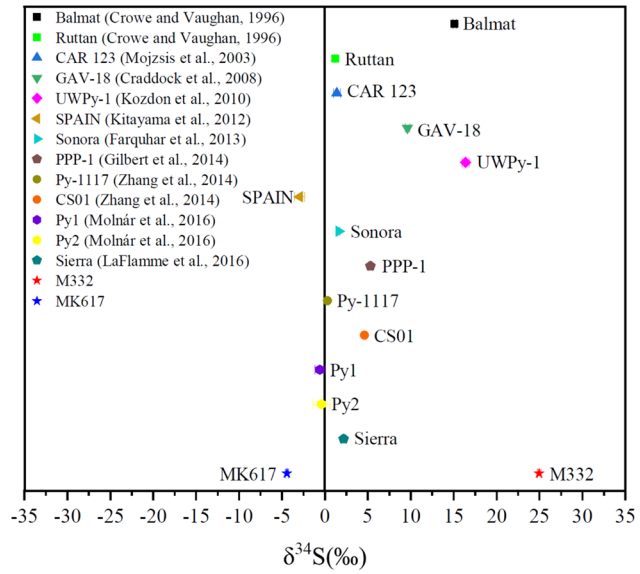

Fig. 5 $\delta^{34}S$ Values in different pyrite reference materials for *in situ* sulfur isotope analysis. Error bars represent ± 2 SD.

$F < F_{critical}$ at a 95% confidence level ($\alpha = 0.05$). All F-values for M332 and MK617 meet this condition, confirming their excellent homogeneity and their suitability as reference materials for *in situ* sulfur-isotope analysis.

3.5 Recommended $\delta^{34}S$ values of M332 and MK617

Homogeneity tests confirm that the $\delta^{34}S$ values are uniform in both M332 and MK617 pyrites. Sulfur isotope compositions, determined by various *in situ* methods across multiple laboratories, are consistent within 2SD uncertainty intervals. For M332, the $\delta^{34}S$ values are 24.86 ± 0.32‰ (SIMS, IGG), 24.58 ± 0.38‰ (SIMS, GIG), 25.20 ± 0.25‰ (NanoSIMS, IGG), and 24.70 ± 0.46‰ (LA-MC-ICP-MS, Wuhan Sample Solution Analytical Technology Co., Ltd). For MK617, the values are −4.33 ± 0.21‰ (LG-SIMS, IGG), −4.60 ± 0.18‰ (LG-SIMS, GIG), −4.21 ± 0.16‰ (NanoSIMS, IGG), and −4.43 ± 0.40‰ (LA-MC-ICP-MS, Wuhan Sample Solution Analytical Technology Co., Ltd). These *in situ* measurements align with bulk sulfur isotope analyses: M332 shows 25.01 ± 0.18‰ (IGG) and 24.90 ± 0.23‰ (ICIER, Nanjing University), while MK617 shows −4.46 ± 0.22‰ (IGG) and −4.40 ± 0.21‰ (ICIER). This consistency validates the accuracy of the sulfur isotope compositions. Therefore, the recommended $\delta^{34}S$ values are 24.96 ± 0.22‰ (2SD, $n = 10$, IRMS) for M332 pyrite and −4.43 ± 0.21‰ (2SD, $n = 12$, IRMS) for MK617 pyrite.

Table 3 ANOVA statistics for homogeneity testing of sulfur isotope compositions of M332 pyrite and MK617 pyrite

		$\nu_{between}$	ν_{within}	$S_{between}^2$	S_{within}^2	F	$F_{critical}$
M332	$^{34}S/^{32}S$	5	128	0.0490	0.0280	1.75	2.29
	$^{33}S/^{32}S$	5	101	0.0518	0.0382	1.36	2.30
MK617	$^{34}S/^{32}S$	5	146	0.0189	0.0124	1.52	2.28
	$^{33}S/^{32}S$	5	117	0.0096	0.0199	0.48	2.29

Compared to existing pyrite reference materials for *in situ* sulfur isotope analysis (Table S7†), M332 and MK617 exhibit a broader sulfur isotope range (Fig. 5), with M332 having the highest and MK617 the lowest $\delta^{34}S$ values.[13,25,26,29–35] This expanded range provides critical support for instrument calibration and method validation, especially in studies involving extreme sulfur isotope compositions. The introduction of M332 and MK617 pyrites fills a critical gap in the availability of reference materials with extreme $\delta^{34}S$ values, enhancing calibration options for researchers studying geochemical or environmental processes. Their high homogeneity and large sample sizes make them ideal for *in situ* techniques such as SIMS and LA-MC-ICP-MS, improving the precision and reliability of microscale analyses.

4. Conclusions

This study demonstrates that M332 and MK617 pyrites exhibit homogeneous sulfur isotope compositions, making them suitable reference materials (RMs) for *in situ* sulfur isotopic analysis such as LG-SIMS, NanoSIMS, and LA-MC-ICP-MS. The recommended $\delta^{34}S$ values, determined by Isotope Ratio Mass Spectrometry (IRMS), are 24.96 ± 0.22‰ (2SD, $n = 10$) for M332 and −4.43 ± 0.21‰ (2SD, $n = 12$) for MK617. Additionally, SIMS analyses provided consistent $\delta^{33}S$ values of 12.89 ± 0.60‰ (2SD, $n = 104$) for M332 and −2.23 ± 0.35‰ (2SD, $n = 120$) for MK617, further validating their reliability. These reference materials provide a broad range of $\delta^{34}S$ values and exceptional homogeneity, addressing the critical need for precise calibration in sulfur isotope research.

Data availability

The datasets generated during and/or analyzed during the current study are available from the corresponding author upon reasonable request.

Author contributions

Jialong Hao: conceptualization, methodology, writing – original draft, supervision and funding acquisition. Ruolong Chi: investigation and validation. Zhengjie Qiu: conceptualization, methodology, writing – review & editing and funding acquisition. Guoqiang Tang: investigation, validation and writing – review & editing. Zexian Cui: investigation, validation and writing – review & editing. Lianjun Feng: investigation, validation and writing – review & editing. Hao Yan: investigation, validation and writing – review & editing. Qiaoqiao Zhu: investigation, validation and writing – review & editing. Ping Gao: validation and visualization. Wei Yang: conceptualization and methodology.

Conflicts of interest

The authors acknowledge that there is no conflict of interest in this article.

Acknowledgements

We thank Xu Tang for Micro-XRF measurement. This study was supported by the Natural Science Foundation of China (42241102, 42173036 and 42372094), and the Scientific Instrument Developing Project of the Chinese Academy of Sciences (Grant no. E1298503).

References

1 J. Farquhar, H. Bao and M. Thiemens, *Science*, 2000, **289**, 756–758.
2 R. R. Seal, *Rev. Mineral. Geochem.*, 2006, **61**, 633–677.
3 L. Marini, R. Moretti and M. Accornero, *Rev. Mineral. Geochem.*, 2011, **73**, 423–492.
4 C. W. Mandeville, *Elements*, 2010, **6**, 75–80.
5 P. R. D. Mason, J. Košler, J. C. M. de Hoog, P. J. Sylvester and S. Meffan-Main, *J. Anal. At. Spectrom.*, 2006, **21**, 177–186.
6 L. Liu, T. R. Ireland and P. Holden, *Geochem. Perspect. Lett.*, 2021, **17**, 45–49.
7 E. H. Hauri, D. Papineau, J. Wang and F. Hillion, *Chem. Geol.*, 2016, **420**, 148–161.
8 N. T. Kita, J. M. Huberty, R. Kozdon, B. L. Beard and J. W. Valley, *Surf. Interface Anal.*, 2011, **43**, 427–431.
9 R. Li, X.-L. Wang, Y. Guan, J. Gu and L.-L. Tian, *J. Anal. At. Spectrom.*, 2023, **38**, 1016–1020.
10 M. J. Whitehouse, *Geostand. Geoanal. Res.*, 2013, **37**, 19–33.
11 Y. Chen, Z. Xie, S. Dong, Q. Lei and J. Gao, *J. Anal. At. Spectrom.*, 2022, **37**, 2529–2536.
12 J.-L. Hao, L.-P. Zhang, W. Yang, Z.-Y. Li, R.-Y. Li, S. Hu and Y.-T. Lin, *Front. Chem.*, 2023, **11**, 1120092.
13 J. Zhang, Y. Lin, W. Yang, W. Shen, J. Hao, S. Hu and M. Cao, *J. Anal. At. Spectrom.*, 2014, **29**, 1934–1943.
14 W. Wang, Y. Hu, A. D. Muscente, H. Cui, C. Guan, J. Hao and C. Zhou, *Geology*, 2021, **49**, 611–616.
15 J. D. Woodhead and J. M. Hergt, *Geostand. Geoanalytical Res.*, 2005, **29**, 183–195.
16 T. R. Ireland, in *Handbook of Stable Isotope Analytical Techniques*, ed. P. A. de Groot, Elsevier, Amsterdam, 2004, pp. 652–691, DOI: **10.1016/B978-044451114-0/50032-6**.
17 L. Martin, P. Guagliardo, W. Rickard and M. Aleshin, in *Treatise on Geochemistry*, ed. A. Anbar and D. Weis, Elsevier, Oxford, 3rd edn, 2025, pp. 829-859, DOI: **10.1016/B978-0-323-99762-1.00108-X**.
18 J.-L. Hao, H.-C. Tian, C. Qi, R.-Y. Li, S. Hu, Y.-T. Lin, Y.-S. He and W. Yang, *Talanta*, 2025, **289**, 127733.
19 J. M. Eiler, C. Graham and J. W. Valley, *Chem. Geol.*, 1997, **138**, 221–244.
20 N. Lv, Z. Bao, K. Chen, C. Zong, Y. Zhang and H. Yuan, *Geostand. Geoanalytical Res.*, 2022, **46**, 451–463.
21 Y. Feng, W. Zhang, Z. Hu, T. Luo, M. Li, Y. Liu, H. Liu and Q. Li, *J. Anal. At. Spectrom.*, 2022, **37**, 551–562.
22 R. K. Rogers and J. H. Davis, *Econ. Geol.*, 1977, **72**, 372–380.
23 W. E. Wilson, J. M. Saul, V. Pardieu and R. W. Hughes, *Mineral. Rec.*, 2009, **40**, 346–407.
24 C. Q. Zhang and J.-H. Li, *At. Spectrosc.*, 2022, **43**, 284–291.
25 J. Farquhar, J. Cliff, A. L. Zerkle, A. Kamyshny, S. W. Poulton, M. Claire, D. Adams and B. Harms, *Proc. Natl. Acad. Sci. U. S. A.*, 2013, **110**, 17638–17643.
26 S. E. Gilbert, L. V. Danyushevsky, T. Rodemann, N. Shimizu, A. Gurenko, S. Meffre, H. Thomas, R. R. Large and D. Death, *J. Anal. At. Spectrom.*, 2014, **29**, 1042–1051.
27 T. Ding, S. Valkiers, H. Kipphardt, P. De Bievre, P. Taylor, R. Gonfiantini and R. Krouse, *Geochem. Cosmochim. Acta*, 2001, **65**, 2433–2437.
28 I. O. f. Standardization, *ISO Guide 35, Reference Materials-Guidance for Characterization and Assessment of Homogeneity and Stability*, International Organization for Standardization, Geneva, 2017.
29 D. E. Crowe and R. G. Vaughan, *Am. Mineral.*, 1996, **81**, 187–193.
30 S. J. Mojzsis, C. D. Coath, J. P. Greenwood, K. D. McKeegan and T. M. Harrison, *Geochim. Cosmochim. Acta*, 2003, **67**, 1635–1658.
31 P. R. Craddock, O. J. Rouxel, L. A. Ball and W. Bach, *Chem. Geol.*, 2008, **253**, 102–113.
32 R. Kozdon, N. T. Kita, J. M. Huberty, J. H. Fournelle, C. A. Johnson and J. W. Valley, *Chem. Geol.*, 2010, **275**, 243–253.
33 Y. Kitayama, E. Thomassot, J. O'Neil and B. A. Wing, *Earth Planet. Sci. Lett.*, 2012, **355–356**, 271–282.
34 F. Molnár, I. Mänttäri, H. O'Brien, Y. Lahaye, L. Pakkanen, B. Johanson, A. Käpyaho, P. Sorjonen-Ward, M. Whitehouse and G. Sakellaris, *Ore Geol. Rev.*, 2016, **77**, 133–162.
35 C. LaFlamme, L. Martin, H. Jeon, S. M. Reddy, V. Selvaraja, S. Caruso, T. H. Bui, M. P. Roberts, F. Voute, S. Hagemann, D. Wacey, S. Littman, B. Wing, M. Fiorentini and M. R. Kilburn, *Chem. Geol.*, 2016, **444**, 1–15.